Summer 2021

Groundwater Discharge From Passive Continental Margins: Rethinking Marine Chemical Budgets

Andrew William Osborne

GROUNDWATER DISCHARGE FROM PASSIVE CONTINENTAL MARGINS: RETHINKING MARINE CHEMICAL BUDGETS

by

Andrew William Osborne

Bachelor of Science
Louisiana State University, 2019

Submitted in Partial Fulfillment of the Requirements

For the Degree of Master of Science in

Geological Sciences

School of the Earth Ocean and Environment

University of South Carolina

2021

Accepted by:

Alicia Wilson, Director of Thesis

Scott White, Reader

Andrew Leier, Reader

Tracey L. Weldon, Interim Vice Provost and Dean of the Graduate School

ACKNOWLEDGEMENTS

The author would firstly like to thank Alicia Wilson for her guidance and knowledgeable insight during the attainment of his degree. He would also like to thank his friends and family for providing the support necessary to maintain a sane mentality during the navigation of academia. Lastly, he thanks Varuzhan Akobian for his excellent and thorough analysis of 1.d4.

ABSTRACT

Geothermal convection and sediment compaction drive large-scale flow in continental shelves. We suggest that this flow is an overlooked control on the major ion chemistry of the ocean. Conventional ocean chemical budgets are constructed using river discharge, axial mid-ocean ridge (MOR) convection and $CaCO_3$ production, but these budgets are still poorly quantified. We synthesized data from 17 passive continental margin basins to calculate a range of estimated groundwater and chemical fluxes from continental shelves, considering five major ions (Ca^{2+}, Na^{+}, K^{+}, Mg^{2+}, and Cl^{-}). When extrapolated globally, volumetric groundwater flux estimates were comparable to those for MOR axial circulation, and our maximum volumetric flux estimates exceeded MORs by ~an order of magnitude. Net chemical fluxes were calculated assuming seawater was the starting composition for groundwater discharging from the basins. Chemical compositions of four likely basinal fluid archetypes were synthesized from the literature. We estimated chemical and groundwater fluxes from passive margins required to close chemical budgets using a mass balance model which also included chemical input from rivers, MORs, and $CaCO_3$ production. We found that passive continental margins have the potential to remove Mg^{2+} from the oceans in a quantity which balances input from the other chemical sources for three out of four considered fluid archetypes. We suggest that passive margins also contribute significant quantities of Ca^{2+} and K^{+} to the oceans, though not in a magnitude large enough to balance chemical budgets on their own.

TABLE OF CONTENTS

LIST OF TABLES

LIST OF FIGURES

CHAPTER 1

INTRODUCTION

Knowledge of major ion chemical budgets of the oceans is necessary for understanding the longevity of marine ecosystems, global carbon budgets, and how marine chemistry changes over geologic time. Despite decades of research, many of these budgets are still uncertain. Major ion budgets of the ocean are thought to be controlled by river discharge, mid-ocean ridge (MOR) hydrothermal convection, off-axis basalt alteration (*Spencer and Hardie,* 1990; *Mottl and Wheat*, 1994; *Stein and Stein,* 1994; *Kadko et al*., 1995; *Schramm et. al.,* 2005), and production and accumulation of calcium carbonate (*Milliman,* 1993; *Locklair and Lerman*, 2005). Rivers contribute net-positive fluxes of cations (Ca^{2+}, Mg^{2+}, Na^{+}, and K^{+}) from weathered continental material in various quantities depending on sediment load and discharge rates. Thermally driven convection of seawater through MOR axes and flanks has been extensively studied for its potential to balance riverine chemical input on a global scale (*Spencer and Hardie*, 1990; *Mottl and Wheat,* 1994; *Elderfield and Shultz,* 1996; *Hardie*, 1996; *Alt*, 2003). MORs have been shown to contribute positive net fluxes of Ca^{2+} and K^{+} and remove Mg^{2+} from the oceans, but the magnitudes of these fluxes are difficult to estimate.

The complexities of determining the rates of MOR heat flux, hydrothermal circulation, and chemical exchange between the different flow regimes have resulted in several different methods used to estimate fluxes, including chemical mass balance (*Spencer and Hardie*, 1990; *Nielson et al*., 2006) and thermal modeling (*Stein and Stein*,

1994), to name only a few of the hundreds of studies done in this field. The consensus is that MORs contribute to marine chemistry in a magnitude which has yet to be confidently constrained or proven to balance riverine input without accounting for one or more additional major sources of chemical input. Similarly, *Milliman* (1993) presented evidence that shallow and deep-water production of calcium carbonates removes Ca^{2+} from ocean water in quantities that exceed input by rivers and MORs, concluding that either the sources and sinks were inaccurate, the oceans were not at steady state, or that there were sources of chemical input not yet identified.

The additional source of chemical input may be found in submarine groundwater discharge (SGD) (*Wilson*, 2003; *Michael et al.*, 2016). SGD refers to the flow of fresh and saline groundwater into the ocean (*Burnett et. al.*, 2002; *Moore*, 2010; *Kwon et al.*, 2014) in coastal areas, here interpreted to include large-scale groundwater flow through continental shelves.

Groundwater migration is widespread in continental shelves (*Aharon et al*., 1992; *Garven*, 1995; *Sanford et al*., 1998; *Jones et al.*, 2000; *Wilson*, 2003, 2005; *Joye*, 2005; *Michael et al.*, 2016). Fresh groundwater is similar to river water in major ion chemistry, and direct discharge of fresh groundwater to the ocean is less than 5% of river discharge over the same catchments (*Befus et al*., 2017). Saline groundwater in sedimentary basins, including continental shelves, is typically significantly altered compared to seawater (*Hitchon and Friedman*, 1969; *Hitchon et al*., 1971; *Manheim and Paull*, 1981; *Hanor*, 1987; *Fisher and Boles*, 1990; *Hardie*, 1991; *Land and Macpherson*, 1992; *Hanor and Macintosh*, 2007). For example, brines in sedimentary basins are commonly enriched in Ca^{2+} and depleted in Mg^{2+} compared to seawater (*Hardie*, 1991). Given the potential

rates at which fluids may be discharging from continental margins (*Kastner et al.*, 1991; *Bekins and Dreiss*, 1992; *Saffer and Bekins*, 2002; *Wilson*, 2003; 2005; *Saffer*, 2015), the chemical impact on the local and global environment may be very significant.

CHAPTER 2

SGD FROM CONTINENTAL MARGINS

2.1 DRIVING FORCES

Several different processes can cause large-scale groundwater migration. On continental land masses, topographic relief, and therefore gravity, is the primary driver of groundwater flow (*Garven*, 1995). In active continental margins, compaction-driven dewatering of accretionary prisms expels fluid from the sediments at rates dependent on sediment permeability and rates of subduction. Quantifying fluid flow in active margins systems is complex, and not fully understood (*Saffer*, 2015). Flow rates have been estimated globally (*Kastner et al.*, 1991) and for individual margins (*Saffer*, 2003; *Moore et al*., 2011), although, as will be shown, the volumetric fluxes are negligible compared to our estimates for flow from passive margins. They also have a global length of coastline which is roughly half that of passive margins (*Mann*, 2014). For these reasons, active margins will not be considered in this study to contribute a significant quantity of saline fluids to the oceans.

In passive continental margins, flow of saline groundwater is controlled primarily by pressure gradients and density gradients (*Garven*, 1995; *Christiansen and Garven*, 2003). Sediment compaction and the concomitant decrease in pore volume create pressure gradients, which become the primary drivers of flow in lower permeability ($k < 10^{-15}$ m^2) continental margins (*Christiansen and Garven*, 2003). Thick layers of compacting sediments often develop overpressures, which are pore pressures that exceed

the hydrostatic pressure at the same depth (*Bethke and Corbet*, 1988; *Harrison and Summa*, 1991; *Garven*, 1995; *Osborne and Swarbrick*, 1997; *Yu and Hilterman*, 2014; *Zhao et al*., 2018). Overpressures can be caused by sediment compaction (*Bethke and Corbet*, 1988) or by the release of excess fluids during conversion of smectite to illite (*Bowers*, 1995; *Zhao et al.*, 2018; *Qin et al.*, 2019) and the generation of hydrocarbons. (*Okiongbo*, 2014). Documented overpressures are a good indicator for flow because they indicate fluid being driven from the sediment, regardless of the origin of the overpressuring. Overpressured basins are common around the world, which suggests that fluid discharge from passive continental margins may contribute significant chemical fluxes to the oceans.

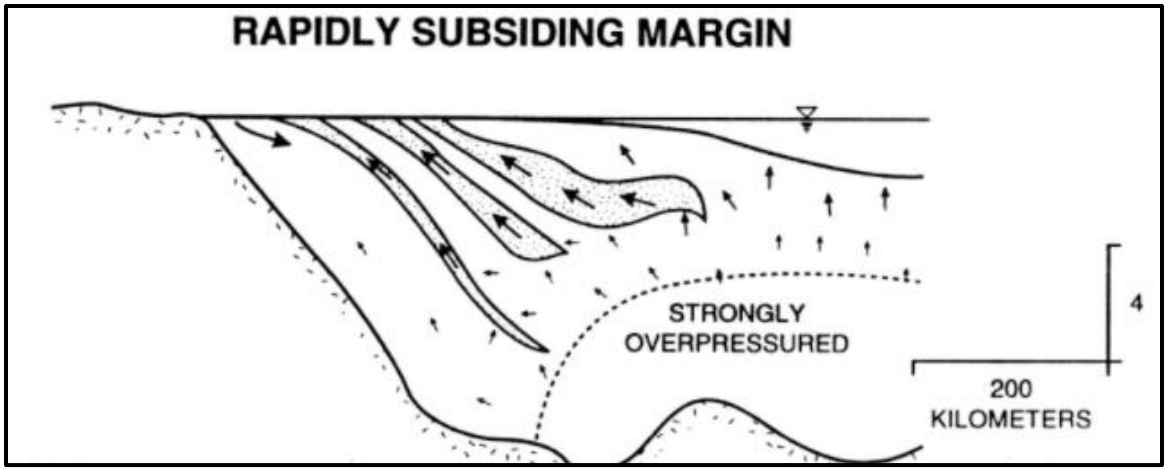

Figure 2.1 Conceptual diagram of compaction driven flow. Modified from *Garven* (1995).

Convection driven by density gradients is the primary mechanism for flow in systems that have a high permeability ($k > 10^{-13}$ m^2) (*Christiansen and Garven*, 2003). Density gradients are created in continental shelves by variations in temperature and salinity (*Wilson*, 2003; 2005). In the case of geothermal convection, density gradients

develop because temperature increases with depth in sedimentary basins, whereas seawater decreases in temperature with depth at a rate dependent on the depth of the thermocline (*NOAA,* 2019; Fig 2.2). Although geothermal convection has been most-often observed or simulated in carbonate platforms, where thermal evidence indicating geothermal convection has been observed (*Kohout*, 1960; *Hardie*, 1987; *Sanford et al.*, 1998; *Jones et. al.*, 2000; *Wilson et. al.*, 2000; *Wilson et al*., 2001), geothermal convection should develop in any setting with a sloping seafloor (*Sanford et al.*, 1998; *Wilson,* 2003).

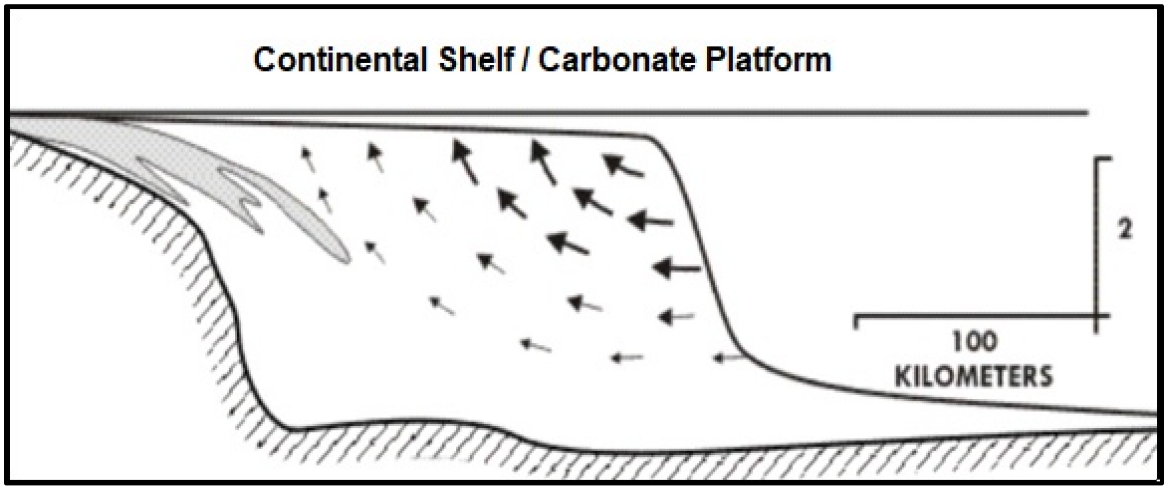

Figure 2.2 Conceptual diagram of geothermal convection in continental shelves and carbonate platforms. Courtesy of *A. M. Wilson*.

Salinity gradients can also drive flow in sedimentary basins, including at the freshwater-saltwater interface (*Michael et al.*, 2016), surrounding salt domes (*Hanor*, 1987), and in reflux systems (*Jones and Xiao*, 2005). However, salinity gradients will not be quantitatively considered in this study due to a lack of evidence for their influence on basin-wide scales.

2.2 CHEMISTRY OF DISCHARGING GROUNDWATER

The chemical composition of groundwater in deep sedimentary basins is commonly significantly altered by chemical processes including mineral dissolution, reprecipitation, and ion exchange (*Drever*, 1997). This results in a chemical difference between the seawater that enters the sediments, whether during initial deposition or due to groundwater flow, and pore fluids that discharge from the basin later (*Fisher and Boles*, 1990; *Land and Macpherson*, 1992). The magnitude of change in chemical composition depends on the local rock type, fluid residence time, temperature, and the original composition of the fluid when it was buried or entered the basin.

Table 2.1 Examples of water-rock reactions that impact the chemistry of groundwater.

Reaction	**Formula**
Dolomitization	$2CaCO_3 + Mg^{2+} \rightarrow CaMg(CO_3)_2 + Ca^{2+}$
Albitization	$CaAl_2Si_2O_8 + 4SiO_2 + 2Na+ \rightarrow 2NaAlSi_3O_8 + Ca^{2+}$
Illitization	Smectite + $K^+ \rightarrow$ illite + $Si^{4+} + Fe^{2+} + Na^+ + Mg^{2+} + nH_2O$

Several varying chemical reactions may occur during sedimentary diagenesis. Dolomitization may occur if carbonates are present in the subsurface. This conversion of calcite to dolomite results in pore fluid that is enriched in Ca^{2+} and depleted in Mg^{2+}. Clay mineral reactions, such as illitization, may occur in shale-rich sedimentary sequences. Illitization occurs around ~100°C – 150°C and causes the clay mineral smectite to release its interlayer water, altering to illite (*Vrolijk*, 1990). This dehydration reaction consumes available K^+ while releasing Mg^{2+} and Na^+ to groundwater. This

process is primarily a function of burial time and formation temperature (*Swarbrick and Osborne*, 1998; *Qin et al*, 2019). Albitization refers to the conversion of existing plagioclase or potassium feldspar to albite and may occur during MOR convection or diagenesis in sedimentary basins. This reaction consumes sodium and increases calcium (or potassium) concentrations in groundwater or hydrothermal fluids. These processes, in combination with the dissolution of evaporites in the subsurface, may result in altered brines that are enriched in Ca^{2+} and K^{+} and depleted in Mg^{2+}, as shown in brines presented by *Hardie* (1991). Examples of brine fluid compositions may be found in Appendix A.

CHAPTER 3

CONCEPTUAL MODEL

Given that groundwater flow is pervasive in passive margin sediments, it is likely that these basins can sustain a significant discharge of fluids with ion concentrations that are markedly different from rivers and ocean water. To assess this possibility, we independently estimated volumetric discharge from overpressured basins likely to generate compaction-driven flow and basins likely to host geothermal convection. We then estimated chemical mass fluxes from these basins assuming different archetypal chemical compositions for the discharging fluids. We then modified the method of *Spencer and Hardie* (1990) to develop a box model that describes the major ion chemistry of the ocean, using modern estimates of volumetric fluxes from axial MOR convection and published mass flux estimates of $CaCO_3$ accumulation. This allowed us to estimate volumetric groundwater discharge from passive continental margins by closing the chemical budget. We then compared our independent volumetric estimates to those generated by the method of *Spencer and Hardie* (1990) to verify them.

Much like previous global-scale studies on the chemical impact of seawater interaction with ocean crust (e.g. *Hart*, 1970; *Thompson*, 1983) this study is designed to provide a first-order estimate of the potential for chemical flux from a previously unexplored source which can be compared to those of the established contributors. The numerous assumptions that must be made to produce any average global-scale estimate create a concomitantly large uncertainty in the calculations. Thus, our results are not

intended to provide a final strictly defined marine chemical budget. Rather, they are meant to begin a discourse on the potential for chemical impact from a source not yet fully understood.

CHAPTER 4

METHODS

4.1 AREAS OF STUDY

17 sedimentary basins in passive continental margins were considered for this study. Each was analyzed for potentially significant groundwater discharge to the oceans due to geothermal convection or compaction-driven flow.

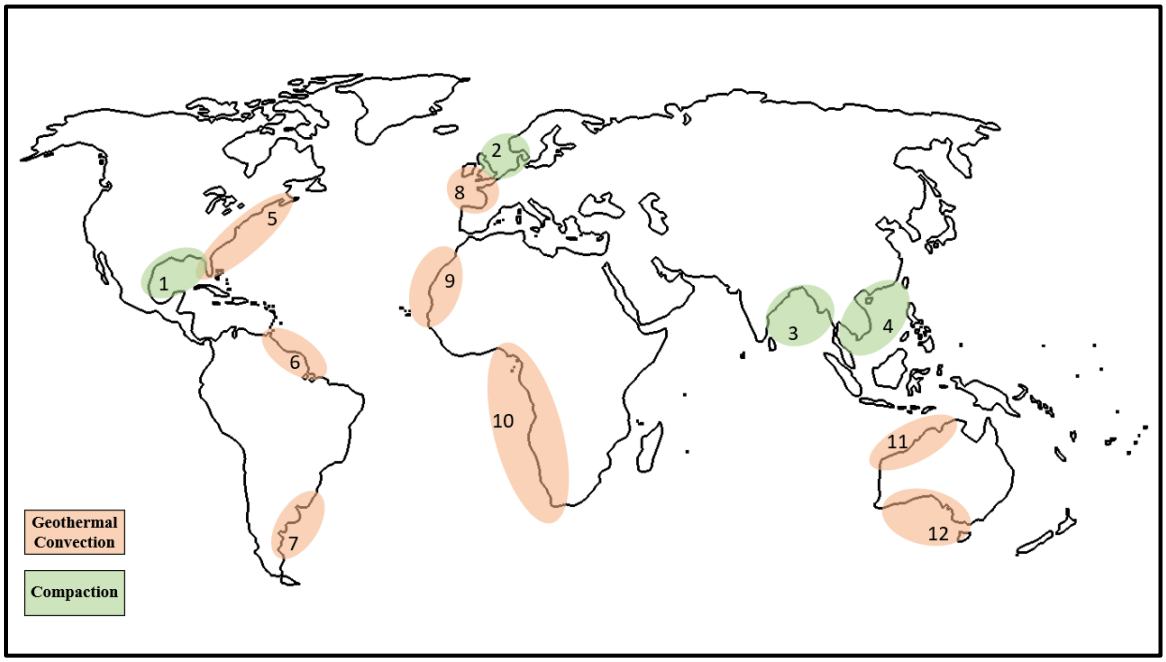

Figure 4.1 Areas of study.
1 – The Gulf of Mexico, 2 –North Sea, 3 – Bengal Basin, *4 – Yinggehai Basin, Nam Con Son Basin, Cuu Long Basin, *5 – N. American East Coast, 6,7 – S. American East Coast, 8 – Celtic Sea, 9,10 – African West Coast, 11 – Great Australian Bight, 12 – N.W. Australian shelf.
* Basins were broken into separate sections and analyzed independently from each other

We assumed that basins whose seafloor geometries resembled those in previous investigations of geothermal convection (*Wilson*, 2003) and were dominated by coarse clastics and carbonates, including carbonate platforms, were subject to geothermal convection (Table 4.1). We chose six basins with literature-verified overpressures (Table 4.2) to estimate compaction-driven flow. These basins are almost entirely composed of clastics, some with shale constituents greater than 90%.

There are 105,000 km of passive margins on earth (*Mann*, 2014). Based on estimates by *Mouchet and Mitchell* (1989) and our own measurements using Google Earth, there are approximately 7.0E+6 km^2 of overpressured submarine sediments along passive margins which account for ~24,000 km of coastline worldwide. We assumed that the remaining ~81,000 km of passive margins had the potential to host geothermal convection. The six basins chosen to estimate compaction-driven flow in this study account for ~23% of the earth's overpressured passive margin area. The 10 margins chosen to estimate geothermal convection in this study represent ~17% of the 81,000 km. Therefore, calculated groundwater fluxes were divided by a factor of .2 to provide an estimate for global groundwater flux, assuming that volumetric fluxes from active continental margins were negligible.

Table 4.1 Basins likely to host geothermal convection.

BASIN	SEDIMENT TYPE	COASTLINE	SOURCE
NW Shelf Australia	Fine Carbonates	2500 km	*Exon et al.* (1982); *Keep et al.* (2007)
Australian Bight	Med. Carbonates	1100 km	*Krassay and Totterdell* (2003)
Celtic Sea	Med. Carbonates	800 km	*Reynaud et al* (1999)
N. America: A[1]	Coarse Clastics	700 km	*Olsson et al.* (1988)
N. America: B[2]	Coarse Clastics	800 km	*Gohn* (1988)
N. America: Florida	Med. Carbonates	600 km	*Scott* (1992)
Africa: A[3]	Fine Carbonates	2100 km	*Leyden et al.* (1972)
Africa: B[4]	Coarse Clastics	1300 km	*Seibold and Hinz*, (1974)
Africa: C[5]	Fine Carbonates	890 km	*Seibold and Hinz* (1974)
S. America: A[6]	Fine Carbonates	1700 km	*Stoakes et al.*(1991); *Sachse et al.* (2016)
S. America: B[7]	Fine Carbonates	1600 km	*Pattier et al.* (2011)

[1] Long Island – Virginia; [2] North Carolina – Georgia; [3] 2°N-17°S; [4] 16°N - 26°N; [5] 31°S-37°S; [6] 33°S - 46°S; [7] 49°W - 59°W

Table 4.2 Basins likely to host compaction-driven flow.

BASIN	AGE (My)	AREA (km^2)	SOURCE
GoM	180	4.4E+5	*Sharp and Domenico*, 1976; *Harrison and Summa*, 1991; *Mello and Karner*, 1996
North Sea	250	5.8E+5	*Mudge and Bujak*, 1994; *Barry et al.*, 2016
Bengal	66	3.2E+4	*Moore et al.*, 1974; *Roy et al.*, 2010*;*
Yinggehai	65	2.2E+5	*Hao et al.*, 1996; *Xinong et al*., 1999; *Luo et al.*, 2003
Cuu Long	25	8.4E+4	*Matthews et al.*, 1997; *Lee et al.*, 2001; *Binh et al.*, 2007;
Nam Con Son	28	2.5E+5	*Lee et al.*, 2001; *Binh et al*., 2007

4.2 GROUNDWATER DISCHARGE FROM COMPACTING BASINS

Total pore-volume loss from the compacting basins was estimated by decompacting the layers in the stratigraphic columns of the six continental shelf complexes in Table 4.2. Decompaction calculations were based on the basins' current thickness, age, and composition. Compaction curves for sand and shale (*Baldwin and Butler*, 1985) (Table 4.3) were applied to each stratigraphic layer, weighted based on the layer's percentage of each component (Eq. 4). The current porosity of each layer at depth was estimated using the equations in Table 4.3. That porosity was "decompacted" to a reasonable initial porosity for each sediment type (60% for shale, 35% for sand), then multiplied by the basin's area to calculate the total volume lost during compaction. This value was divided by the age of the basin, thereby giving a flux of groundwater since initial deposition. Basin areas were estimated using measurements from previous studies (Table 4.2), where only the offshore areas were considered for contributary relevance. A range of possible fluid discharges was produced for each continental shelf complex by performing separate calculations using upper and lower bound values for the shale fraction in each layer. We believe estimating the area and the porosity at depth introduce uncertainties of a factor of two each. Therefore, the upper and lower bound fluxes for each basin were averaged, then multiplied and divided by a factor of four to generate minimum and maximum flux values. Calculating the discharge this way results in an average flux over time, so basins that were compacting more rapidly in the geologic past overestimate current annual volumetric fluxes.

Although this introduces some additional uncertainty into our calculations, the annual flux from geothermal convection proved to be much more significant to the global chemical budget, reducing the impact of this assumption on our results.

Table 4.3 Compaction curves based on *Baldwin and Butler* (1985)[a]

Lithology	Porosity
Shale > 200 m	$\phi = 1 - \sqrt[6.35]{d/6.02}$
Shale < 200 m	$\phi = 1 - \sqrt[8]{d/15}$
Sandstone	$\phi = {0.49}/{e^{(\frac{d}{3.7})}}$

[a] Curves were modified to solve for porosity (ϕ) as a function of burial depth (d) in stratigraphic sequences of known compositions.

The original thickness (m) was calculated according to:

$$b_o = X_{sh}\frac{\phi_{sh}(z)*b}{\phi_{sh(o)}} + X_s\frac{\phi_s(z)*b}{\phi_{s(o)}} \quad \textbf{(1)}$$

where $\boldsymbol{b_o}$ is the original thickness of the layer, $\boldsymbol{X_{sh}}$ is the percent shale composition of the layer, $\boldsymbol{\phi_{sh}(z)}$ is the porosity of shale at the depth of the layer, $\boldsymbol{b}$ is the current thickness of the layer, $\boldsymbol{\phi_{sh(o)}}$ is the original porosity of shale at deposition, $\boldsymbol{X_s}$ is the percent sand composition of the layer, $\boldsymbol{\phi_s(z)}$ is the porosity of sand at the depth of the layer, and $\boldsymbol{\phi_{s(o)}}$ is the original porosity of sand.

This process was repeated for every layer in the stratigraphic column and summed to get the total original thickness. Fracturing in the sediment column was not mathematically considered because it does not affect the volume of the sediment. Cases of basin inversion and unconformities in the sedimentary record were also not considered in the calculations because sediments would not be compacting during times of uplift, so they would not be discharging fluids in quantities relevant to our study. The total annual flux of discharging groundwater ($\boldsymbol{Q_t}$) for each basin can be calculated by the following equation:

$$\boldsymbol{Q_t} = \frac{(\boldsymbol{b_o} - \boldsymbol{b}) * \boldsymbol{A}}{\boldsymbol{dt}} \quad \textbf{(2)}$$

where $\boldsymbol{A}$ is the basin's area and $\boldsymbol{dt}$ is the basin's age.

4.3 COMPILATION OF GROUNDWATER FLUXES CAUSED BY GEOTHERMAL CONVECTION

Density-driven fluxes were estimated based on *Wilson* (2003), who used numerical models to estimate a range of possible groundwater fluxes due to geothermal convection using the bathymetry of North American continental shelves. Wilson used realistic seafloor geometries for seven cross sections and reported a range of fluxes representative of five composite rock types. The range of values for each representative lithology were averaged by taking a geometric mean. The dominant lithology of each shelf complex considered in this study was estimated from published cross sections, and the averaged representative flux value from *Wilson* (2003) was assigned to each basin and multiplied by the length of the coastline. This value was multiplied and divided by a

factor of five to account for the uncertainty in estimating a single lithology for a shelf complex. This gives minimum and maximum flux values which vary by ~an order of magnitude for each basin.

4.4 CHEMICAL FLUXES

To constrain the chemical impact of passive margins, the composition of discharging fluids must be defined. Compositions of different saline fluids observed in continental shelves with trends representative of various sedimentary environments were gathered from the literature and separated into four basic types, hereafter referred to as groundwater archetypes (Table 4.4).

The first fluid archetype represents cold seeps, a global phenomenon of seepage of volatile elements and fluids from the seafloor. Cold seep fluids typically react with rocks at relatively low temperatures, below ~100°C. They vary in composition and flow pattern depending on the character of the sedimentary environment (*Suess*, 2014). We developed a representative composition for cold seeps based on brine pools observed in the Gulf of Mexico (GoM) (*Aharon et al.*, 1992; *Van Cappellen et al.*, 1998; *Joye et al.*, 2005). They are enriched in K^+ and Na^+, depleted in Ca^{2+} and Mg^{2+}, and have a high chlorinity (103,000 mg/l) relative to seawater. These fluids differ from cold seeps observed in convergent margins, which are typically depleted in K^+ via such reactions as the smectite-illite transition (Kastner, 1991).

The second archetype represents fluids in basins dominated by clastic sediments. We averaged the concentrations of eight samples from the New Jersey continental shelf (*IODP* 313, Site M0027) and 14 samples from the San Joaquin Basin (*Fisher and Boles*, 1990). These fluids show similar chemical trends, and we believe them to be

representative of fluids in clastic-dominated passive margins. These fluids have low average chlorinities (~16000 mg/l), possibly due to dilution by fresh groundwater or illitization. They are enriched in Ca^{2+}, and depleted in K^{+}, Mg^{2+}, and Na^{+}. It is worthy to note that fluids sampled from the Nankai Trough (*Taira et al*., 1991; *IODP* 131, Hole 808B), a convergent margin also dominated by clastics, showed similar trends in Mg^{2+} and K^{+} but were depleted in Ca^{2+}. They were not included in this study as they are not representative of fluids from a coastal marine basin, although they are a potential representation of fluids discharging from active margins.

The third fluid archetype was modeled after deep basinal $CaCl_2$ brine fluids (Table 8 *Hardie*, 1991), also known as oil-field brines. These fluids are representative of high chlorinity (182,000 mg/l), high density, evaporite-derived fluids with long residence times at elevated temperatures (>80 °C). The composition of the archetype is an arithmetic average of samples from the GoM (Table 13 *White et al*., 1963; *Carpenter et al*., 1974), the Illinois Basin (*Graf et al*., 1966), the Michigan Basin (*Graf et al*., 1966), and the Dead Sea (*Bentor*, 1969). Fluids are enriched in Ca^{2+} and K^{+} and depleted in Mg^{2+} and Na^{+}. Original fluid compositions can be found in Appendix D.

The final fluid archetype was created by averaging ion concentrations of four samples (depths ~350-410 mbsf) from the Great Australian Bight (*Feary et al.*, 2000). They are moderate chlorinity (55,300 mg/l) fluids enriched in Ca^{2+} and Na^{+} and depleted in Mg^{2+} and K^{+}. Samples from shallower sections show the same trends. Salinities are ~three times higher than seawater (~100,000 mg/l), suggesting evaporation or interaction with evaporite sequences. The trends for Ca^{2+}, Mg^{2+}, and K^{+} are consistent with those of warm spring samples from the Floridian platform (*Fanning et al*., 1981), though these

samples are slightly depleted in Na^+ and have a salinity roughly equal to seawater. Based on the similar trends, we chose the Great Australian Bight samples to represent carbonate-derived fluids.

Table 4.4 Groundwater compositions of seawater, rivers, MORs, and groundwater archetypes.

CONCENTRATIONS (mg/l)	**Ca^{2+}**	**K^+**	**Mg^{2+}**	**Na^+**	**Cl^-**	**Source**
Seawater	412	403	1300	1080	19400	*Riley and Chester* (1971)
Cold Seeps	1370	2580	685	60800	1.03E+5	Foot note [a]
Clastic-Derived	1520	124	59.2	6520	11200	*Fisher and Boles* (1990)
Deep $CaCl_2$ Brines	45300	8270	6680	48200	1.82E+5	*Hardie* (1991) [b]
Carbonate-Derived	1760	1040	2763	32200	55300	*Feary et al*. (2000)
Modified Cold Seeps	-153	86.3	-1170	717	0	-
Modified Clastic-Derived	877	-134	-732	-550	0	-
Modified Deep $CaCl_2$ Brines	4420	480	-582	-5650	0	-
Modified Carbonate-Derived	204	-37.7	-325	509	0	-
Modified MORs	1160	1100	-1280	-907	0	*Spencer and Hardie* (1990)
Modified Rivers	13.2	1.29	2.97	1.95	0	*Spencer and Hardie* (1990)

Concentrations were modified from original sources according to the method of *Spencer and Hardie* (1990).
a. *Aharon et al.* (1992); *Van Cappellen et al*. (1998); *Joye et al*. (2005)
b. Table 8 in *Hardie* (1991).

We calculated net chemical fluxes for each input fluid based on the assumption that the net chloride flux is zero (*Spencer and Hardie*, 1990). We first adjusted the compositions of all input fluids to zero chloride by subtracting ions in proportion to the composition of modern seawater (*Riley and Chester*, 1971). This approach assumes that

seawater-derived salt aerosols dissolved in rainwater are the source of chloride in river waters (*Spencer and Hardie*, 1990), that seawater was the original source water for hydrothermal brines and for our groundwater archetypes. Details of this process are included in Appendix B.

Net chemical fluxes from passive continental margins were calculated by multiplying the concentration of each archetype by the minimum and maximum groundwater flux estimates to generate a mass flux (kg/yr) for each ion. The mass fluxes generated using this method represent endmembers in a range of possible groundwater compositions, as they each assume total discharge is representative of only one archetype. River chemical mass fluxes were gathered from *Spencer and Hardie* (1990). MOR chemical mass fluxes were synthesized using a hydrothermal brine composition from borehole #8, Reykjanes, Iceland, given by *Bjornson* et al. (1972) (the same brine composition used by *Spencer and Hardie*, 1990). We chose the MOR axial fluid flux presented by *Nielsen et al.* (2006), as it fell in a range whose upper bounds agreed with the heat flow estimates of *Mottl and Wheat* (1994). Removal of ions due to precipitation of carbonates assumed a formula for high-Mg calcite of $(Ca_{0.9,}Mg_{0.1})CO_3$ (*Althoff*, 1977), and a total carbonate accumulation of 3 billion tons per year (*Milliman*, 1993). We have not included estimates for mass fluxes from MOR flanks as they are not well constrained; estimates for flank fluxes from various papers (compiled in Table 1 of *Alt*, 2003) predict values for individual ions which vary by up to three orders of magnitude. Mass fluxes from MOR flanks are likely significant for Mg^{2+} (*Alt et al*., 1996; *Nielson*, 2006), though fluxes of other major ions are unclear.

4.5 BOX MODEL OF MARINE CHEMISTRY

A mass balance model was constructed to analyze ocean chemistry based on the following equation:

$$\boldsymbol{Q_{mor}C_{mor} + Q_rC_r + Q_sC_s + m_C = 0} \quad \textbf{(3)}$$

where $\boldsymbol{Q_{mor}}$ is the volumetric flux of hydrothermal fluid through MORs, 6.54e+9 m^3/yr (*Nielson et al*., 2006), $\boldsymbol{C_{mor}}$ is the adjusted concentration of hydrothermal fluids (*Spencer and Hardie*, 1990), $\boldsymbol{Q_r}$ is the global volumetric river discharge, 3.75e+13 m^3/yr (*Spencer and Hardie*, 1990), $\boldsymbol{C_r}$ is the adjusted concentration of river water (*Spencer and Hardie*, 1990), $\boldsymbol{Q_s}$ is the theoretical volumetric flux of groundwater from passive margins required to balance chemical input from rivers and MORs, $\boldsymbol{C_s}$ is the archetypal composition of the discharging groundwater, and $\boldsymbol{m_C}$ is the removal of calcium carbonate, -1.06E+12 kg/yr Ca^{2+} and -7.15E+10 kg/yr Mg^{2+} (based on *Milliman*, 1993). This approach assumes that ocean chemistry is at steady state. If groundwater composition can be estimated, Equation 3 can be rearranged to solve for $\boldsymbol{Q_s}$.

We first tested our model to ensure that it could replicate the results of *Spencer and Hardie* (1990). Thereafter we updated the model to use an updated volumetric hydrothermal fluid flux through MORs (*Nielsen et al.*, 2006) and used Equation 3 to calculate $\boldsymbol{Q_s}$ for each ion from each archetypal composition. Unit conversions were performed assuming a fluid density of 1100 kg/m^3. Some of the possible net ion concentrations have a sign that increases the budget deficit for that ion, so a "theoretical required flux" cannot be calculated for those concentrations.

We compared our globally extrapolated independent estimates to those calculated using Equation 3 using the following equation:

$$\boldsymbol{Q_f = \frac{Q_i}{Q_s}} \quad \textbf{(4)}$$

where $\boldsymbol{Q_f}$ is the flux ratio (Table 6.1) and $\boldsymbol{Q_i}$ is our globally extrapolated independent volumetric groundwater discharge estimate.

We also calculated a theoretical groundwater composition (Table 5.2) which would balance the input from MORs and rivers using our global independent volumetric estimates:

$$\boldsymbol{C_{th} = \frac{(Q_{mor}C_{mor})+(Q_rC_r)}{Q_i}} \quad \textbf{(5)}$$

where $\boldsymbol{C_{th}}$ is the theoretical average groundwater composition in passive margins expressed as the modified net addition/subtraction to seawater in mg/l, as in (Table 4.4). This calculation was repeated for each ion.

CHAPTER 5

RESULTS

Volumetric groundwater fluxes calculated for individual overpressured basins ranged from as low as 1.38E+6 m^3/yr to 2.28E+8 m^3/yr (Figure 5.1). The fluxes varied between basins according to the areal extent of the offshore area, age, and the percent shale component of the sedimentary record. For example, the area of the GoM is slightly smaller than that of the North Sea (Table 4.2) yet has a much higher estimated volumetric flux due to its higher shale component. The Nam Con Son Basin has a relatively low shale component but has been actively compacting throughout its short (Table 4.2) history.

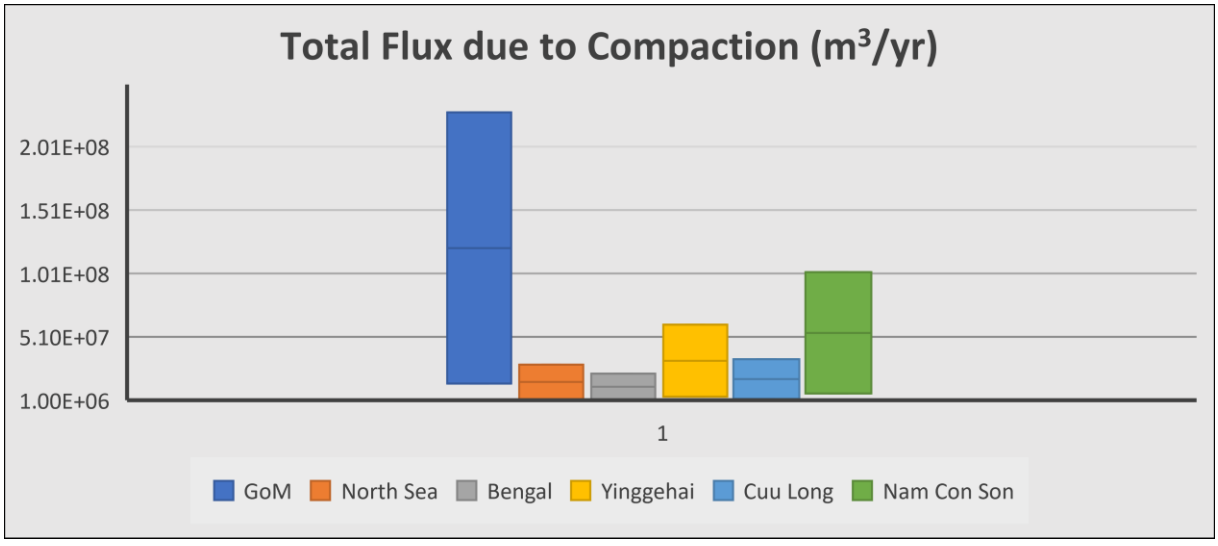

Figure 5.1. Calculations of groundwater flux from individual basins using the decompaction method.

Estimates for volumetric discharge due to geothermal convection in individual basins ranged from 7.26E+06 m^3/yr to 3.57E+09 m^3/yr (Figure 5.2). Fluxes varied predictably according to the dominant sediment type and length of the coastline, though the former was far more impactful on the result. The maximum estimate for each basin is about ~20x higher than the corresponding minimum.

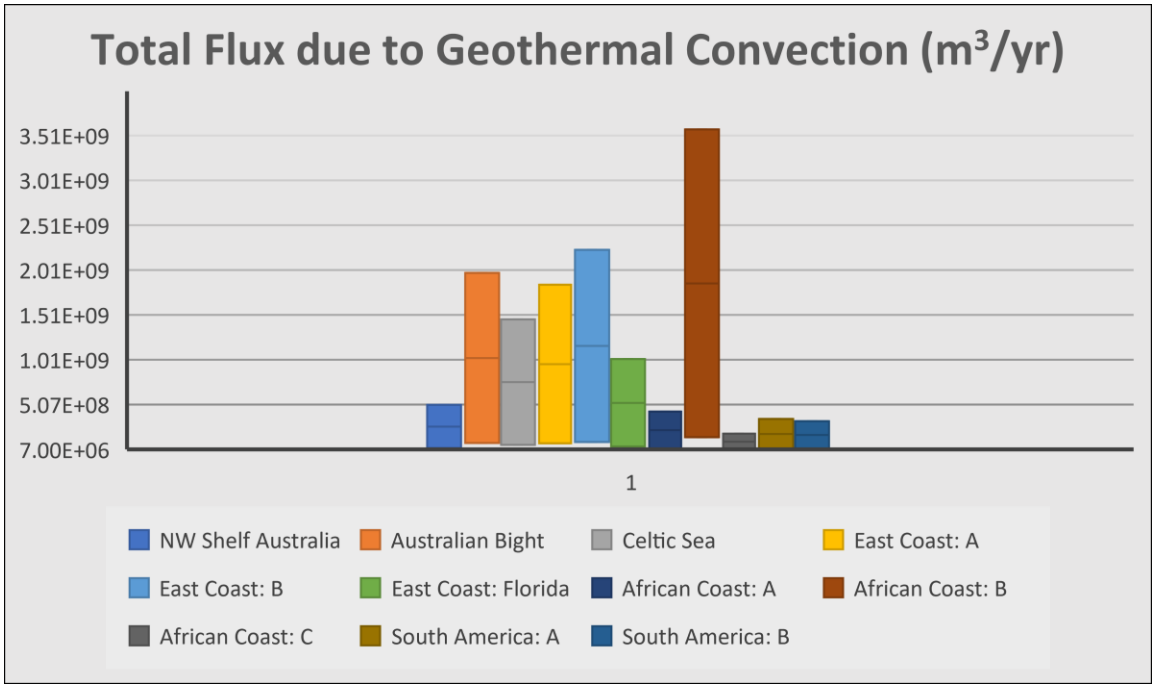

Figure 5.2 Calculations of groundwater flux (m^3/yr) from individual basins assuming geothermal convection as the driving force.

The total minimum volumetric flux due to geothermal convection (5.55E+08 m^3/yr) was ~20x larger than the minimum flux for compaction (2.97E+07 m^3/yr), and the total maximum flux of geothermal convection (1.39E+10 m^3/yr) was ~2x larger than the maximum for compaction driven flow (4.75E+08 m^3/yr). The total globally extrapolated volumetric flux from passive margins ($\boldsymbol{Q_i}$) ranges from 5.85E+08 m^3/yr to 1.44E+10 m^3/yr. Estimated volumetric fluxes of axial MOR convection (6.54E+9 m^3/yr) (*Nielson et*

al., 2006) falls within this range. Estimated river discharge (3.75E+13 m^3/yr) (*Spencer and Hardie,* 1990) is much larger than our estimates.

The mass flux calculations revealed maximum fluxes that exceed MOR contributions for most ions (Table 5.1). Different archetypes show the potential for positive and negative mass fluxes of each ion with the exception of Mg^{2+}, which shows a negative mass flux for every archetype. The combined input from rivers, MORs, and $CaCO_3$ precipitation gives a net positive mass flux of all ions except Ca^{2+}. Therefore, positive archetypal concentration values for Mg^{2+}, Na^+, and K^+ cannot close the budget, regardless of the magnitude of volumetric flux from passive continental margins. The same is true for the single negative concentration value of Ca^{2+}.

Table 5.1 Estimated global upper bound ionic mass fluxes for the four fluid archetypes from passive continental margins and ionic mass fluxes of MORs, rivers, and accumulation of $CaCO_3$ (kg/yr).

	Ca^{2+}	**K^+**	**Mg^{2+}**	**Na^+**
Cold Seeps	-1.10E+10	6.19E+09	-8.37E+10	5.14E+10
Clastic-Derived	6.30E+10	-9.62E+09	-5.25E+10	-3.95E+10
Deep $CaCl_2$ Brines	3.17E+11	3.45E+10	-4.18E+10	-4.06E+11
Carbonate-Derived	1.47E+10	-2.70E+09	-2.34E+10	3.66E+10
MORs	7.60E+09	7.19E+09	-8.37E+09	-5.90E+09
Rivers	4.98E+11	4.84E+10	1.11E+11	7.33E+10
$CaCO_3$	-1.06E+12	0	-7.15E+10	0

Lower-bound global estimates can be found in Appendix C.

The theoretical average concentration of groundwater in passive margins $\boldsymbol{C_{th}}$, calculated by Equation 5, predicts negative concentrations of K^+, Mg^{2+}, and Na^+ and a

positive concentration of Ca^{2+} (Table 5.2). These values are calculated using our estimates for volumetric discharge of groundwater from passive margins and assume that there are no unidentified sources or sinks of chemical input which contribute to marine chemistry. The result does not explicitly include chlorinity, as per limitations of the methods used to adjust the original compositions of fluids, though the method implies a Cl^- equal to seawater.

Table 5.2 Estimated theoretical average concentration of groundwater discharging from passive continental margins expressed as a net difference from its adjusted original source (mg/l).

	Ca^{2+}	K^+	Mg^{2+}	Na^+
Max Estimate	1.9E+05	-1.9E+04	-1.1E+04	-2.3E+04
Min Estimate	7800	-770	-440	-940

CHAPTER 6

DISCUSSION

Our results suggest that groundwater flow through passive continental margins has a significant impact on the major ion chemistry of the ocean. Based on our estimated volumetric discharge rates and archetypal compositions of groundwater likely to be observed in passive margins, the magnitude of the geochemical flux from passive continental margins compares to that of axial fluid circulation through MORs for all considered ions.

Table 6.1 Volumetric flux (m^3/yr) required to balance riverine and MOR chemical input for each groundwater archetype based on equation 3.

	Cold Seeps	**Clastic-Derived**	**$CaCl_2$ Brines**	**Carbonate-Derived**
		REQUIRED FLUX		
1 – Na^+	-	1.2E+11	1.2E+10	-
2 – Mg^{2+}	2.7E+10	4.3E+10	5.4E+10	9.6E+10
3 – Ca^{2+}	-	6.3E+11	1.3E+11	2.7E+12
4 – K^+	-	4.2E+11	-	1.5E+12
		FLUX RATIO [a]		
5 – Na^+	-	1.71	0.17	-
6 – Mg^{2+}	0.37	0.60	0.76	1.3
7 – Ca^{2+}	-	8.8	1.8	38
8 – K^+	-	5.8	-	21

a. Ratio (Equation 4) of the maximum global volumetric flux estimate from independent basin analyses (7.2E+10 m^3/yr) to the volumetric flux for each archetype calculated by the mass balance model (Lines 1—4). Flux Ratios for the minimum global volumetric estimate (2.9E+09 m^3/yr) can be found in Appendix C.
Dashed cells indicate an ion concentration that cannot close the budget.

Three groundwater archetypes may close the Mg^{2+} budget assuming a volumetric flux within the range of our estimates (Table 6.1), and the fourth (Carbonate-Derived Fluid) gives a required volumetric flux which is within ~30% of our maximum. Keeping in mind that these are only endmember compositions, and that the average composition of groundwater is likely more similar to the concentration presented in Table 5.2, it is encouraging that Mg^{2+} trends negatively in all of the fluids presented. The intriguing similarity of this average global composition to chemical trends given for the Clastic-Derived Fluids, suggests that the flux from clastic-dominated margins may be more significant than that from carbonate platforms on a global scale. We note, however, that we have only analyzed five major ions in this study. Other common ions in groundwater such as SO_4^{2-} and HCO_3^- may not correlate as closely.

Although the results of the mass balance model suggest that passive margins likely hold significance in the marine chemical budget, we do not suggest that it is the "final piece" of this global puzzle. There are very likely other undiscovered or underestimated sources of chemical flux. K^+ is not well-balanced by our model; flux ratios range from ~5—500, suggesting that one or more additional sinks are necessary to close the K^+ budget. Low temperature alteration of seafloor basalts on ridge flanks has been suggested (*Hart and Staudigel*, 1982; *Alt, et al*., 1996; *Alt*, 2003), but the magnitude of this impact on a global scale is still poorly defined. The possibility that both processes may play an important role complements the results of *Hart and Staudigel* (1982), who suggested that K^+ not removed from the oceans by alteration of the seafloor was likely removed by continental shelf sediments. The calcium budget is also difficult to balance without assuming a very high average concentration in groundwater (Table 5.2) and our

maximum volumetric estimates from passive margins. Echoing the conclusions of *Milliman* (1993), this could suggest either other Ca^{2+} sources in the established literature are underestimated, the massive sink of $CaCO_3$ accumulation (~2x riverine input of Ca^{2+}) is overestimated, there are additional sources of Ca^{2+} we have not considered, or marine chemistry is not steady state.

The formatting of marine chemical mass-balance models to fit a steady state process is a potentially erroneous assumption which has been adopted by many studies in addition to our own. It is not unreasonable to suggest that there is a net loss or gain of any ion in the oceans over geologic time. This idea has been the studied extensively over the last few decades (*Hardie*, 1996; 2003; *Müller et al.,* 2013). Precisely quantifying the fluxes that would be needed to create a comprehensive transient box model of ocean chemistry is not currently feasible, but the results of our study provide an interesting development in the process of determining the cause and rate of change of marine chemistry.

Some basins in this study are undoubtedly more complex than presented here, which, upon closer examination, may result in much lower (or higher) volumetric fluxes than we have predicted with our relatively simple, globally averaged models. If the true measure of volumetric groundwater flux through continental margins is closer to our minimum estimate, we may conclude that the chemical impact is relatively insignificant compared to the established sources (rivers, MORs, $CaCO_3$ production). However, we believe the magnitude of our maximum estimates are significant enough to warrant further inquiry into the subject.

Future case studies on specific basins may result in better physical constraints on volumetric flux for both driving forces presented in this study, in addition to the accumulation of data that may support analyses of basins that host similar sedimentary features.

CHAPTER 7

CONCLUSIONS

Passive continental margins have the potential to significantly influence marine chemistry. The calculated global volumetric fluxes combined with the archetypes chosen to represent fluids in passive margins produce a range of mass fluxes, the upper range of which compare to or exceed the magnitude of thermally driven seawater circulation at MOR axes for all considered ions. The groundwater flux estimates determined via our steady-state mass balance model and fluid archetypes compared to our independent global volumetric estimates in varying degrees. Notably consistent are the Flux Ratios presented for Mg^{2+}, which suggest that the flux of Mg^{2+} required to balance the budget falls within our predicted range for three out of four fluid archetypes. Budgets for Ca^{2+} and K^{+} may only be partially balanced using our models, suggesting that either the sources of chemical input are inaccurate, there are unconsidered sources of chemical input, or that marine chemistry is not a steady-state system.

The groundwater archetypes considered, while modeled after field samples, are not comprehensive examples of the possible ion concentrations that exist in nature. The average global concentration of groundwater discharging from passive continental margins could potentially match chemical trends for the Clastic-Derived Fluid archetype. Our results are intended as a first-order global estimate for the chemical impact of passive continental margins and consequently include a significant amount of uncertainty.

However, if the true value of global mass flux through passive margins reflects the upper range of our estimates, then these fluxes are significant to the marine chemical budget and should be included in future studies.

WORKS CITED

1. Aharon, P., Roberts, H. H. & Snelling, R. Submarine venting of brines in the deep Gulf of Mexico: Observations and geochemistry. *Geology* **20**, 483–486 (1992).
2. Alt, J. C. Hydrothermal fluxes at mid-ocean ridges and on ridge flanks. *Comptes Rendus Geoscience* **335**, 853–864 (2003).
3. Alt, J. C. *et al. Ridge flank alteration of upper ocean crust in the eastern Pacific: A synthesis of results for volcanic rocks of holes 504B and 896A*. vol. 148 (Ocean Drilling Program, College Station, TX, 1996).
4. Althoff, P. L. Structural refinements of dolomite and a magnesian calcite and implications for dolomite formation in marine-environment. *American Mineralogist* **62**, 772–783 (1977).
5. Baldwin, B. & Butler, C. O. Compaction Curves. *AAPG Bulletin* **69**, 622–626 (1985).
6. Barry, P. H. *et al.* Noble gases solubility models of hydrocarbon charge mechanism in the Sleipner Vest gas field. *Geochimica et Cosmochimica Acta* **194**, 291–309 (2016).
7. Befus, K. M., Kroeger, K. D., Smith, C. G. & Swarzenski, P. W. The Magnitude and Origin of Groundwater Discharge to Eastern U.S. and Gulf of Mexico Coastal Waters: U.S. East Coast Groundwater Discharge. *Geophys. Res. Lett.* **44**, 10,396-10,406 (2017).

8. Bekins, B. A. & Dreiss, S. J. A simplified analysis of parameters controlling dewatering in accretionary prisms. *Earth and Planetary Science Letters* **109**, 275–287 (1992).
9. Bentor, Y. K. On the evolution of subsurface brines in Israel. *Chemical Geology* **4**, 83–110 (1969).
10. Bethke, C. M. & Corbet, T. F. Linear and nonlinear solutions for one-dimensional compaction flow in sedimentary basins. *Water Resour. Res.* **24**, 461–467 (1988).
11. Binh, N. T. T., Tokunaga, T., Son, H. P. & Van Binh, M. Present-day stress and pore pressure fields in the Cuu Long and Nam Con Son Basins, offshore Vietnam. *Marine and Petroleum Geology* **24**, 607–615 (2007).
12. Bischoff, J. L. & Dickson, F. W. Seawater-basalt interaction at 200°C and 500 bars: Implications for origin of sea-floor heavy-metal deposits and regulation of seawater chemistry. *Earth and Planetary Science Letters* **25**, 385–397 (1975).
13. Bjornsson, S., Arnorsson, S. & Romasson, J. Economic evaluation of Reykjanes thermal brine area, Iceland. *Bulletin of American Petrology and Geology* **56**, 2380–2391 (1972).
14. Bowers, G. L. Pore Pressure Estimation from Velocity Data: Accounting for Overpressure Mechanisms Besides Undercompaction. in *SPE Drilling and Completion* 89–95 (Society of Petroleum Engineers, 1995).
15. Burnett, B. *et al.* Assessing methodologies for measuring groundwater discharge to the ocean. *Eos Trans. AGU* **83**, 117 (2002).

16. Carpenter, A. B., Trout, M. L. & Pickett, E. E. Preliminary report on the origin and chemical evolution of lead and zinc-rich oil field brines in central Mississippi. *Economic Geology* **69**, 1191–1206 (1974).
17. Charlou, J. L., Donval, J. P. & Zitter, T. Evidence of methane venting and geochemsitry of brines on mud volcanoes of the eastern Mediterranean Sea. *Oceanographic Research Papers* **50**, (2003).
18. Christiansen, L. B. & Garven, G. A theoretical comparison of buoyancy-driven and compaction-driven fluid flow in oceanic sedimentary basins: THEORETICAL COMPARISON. *J. Geophys. Res.* **108**, (2003).
19. Drever, J. I. *The Geocehmistry of Natural Waters: Surface and Groundwater Environments.* (Prentice Hall, 1997).
20. Eder, W., Schmidt, M. & Koch, M. Prokaryotic phylogenic deversity and corresponding geochemical data of the brine/seawater interface of the Shaban Deep, Red Sea. *Environmental Microbiology* **4**, 758–763 (2002).
21. Elderfield, H. & Schultz, A. Mid-Ocean Ridge Hydrothermal Fluxes and the Chemical Composition of the Ocean. *Annu. Rev. Earth Planet. Sci.* **24**, 191–224 (1996).
22. Exon, N. F., Von Rad, U. & Von Stackelberg, U. The geological development of the passive margins of the Exmouth Plateau off northwest Australia. *Marine Geology* **47**, 131–152 (1982).
23. Fanning, K. A. *et al.* Geothermal springs of the West Florida continental shelf: Evidence for dolomitization and radionuclide enrichment. *Earth and Planetary Science Letters* **52**, 345–354 (1981).

24. Feary, D. A., Hine, A. C. & Malone, M. J. Shipboard Scientific Party. Site 1126. in *Proc. ODP, Init. Repts*. vol. 182 1–110 (2000).

25. Fisher, J. B. & Boles, J. R. Water—rock interaction in Tertiary sandstones, San Joaquin basin, California, U.S.A.: Diagenetic controls on water composition. *Chemical Geology* **82**, 83–101 (1990).

26. Garven, G. Continental-Scale Groundwater Flow and Geologic Processes. *Annual Review of Earth and Planetary Sciences* **23**, 89–117 (1995).

27. Gohn, G. S. Late Mesozoic and early Cenozoic geology of the Atlantic Coastal Plain: North Carolina to Florida. in *The Atlantic Contientnal Margin* (1988).

28. Graf, D. L., Meents, W. F., Friedman, I. & Shimp, N. F. The origin of saline formation waters, III. Calcium chloride waters. *Illinois State Geological Survey* **397**, 60 (1966).

29. Hanor, J. S. & Mcintosh, J. C. Diverse origins and timing of formation of basinal brines in the Gulf of Mexico sedimentary basin. *Geofluids* **7**, 227–237 (2007).

30. Hanor, J. S. Kilometre-scale thermohaline overturn of pore waters in the Louisiana Gulf Coast. *Nature* **327**, 501–503 (1987).

31. Hao, F., Li, S., Sun, Y. & Zhang, Q. Characteristics and origin of the gas and condensate in the Yinggehai Basin, offshore South China Sea: evidence for effects of overpressure on petroleum generation and migration. *Organic Geochemistry* **24**, 363–375 (1996).

32. Hardie, L. A. On the Significance of Evaporites. *Annual Review of Earth and Planetary Sciences* **19**, 131–168 (1991).

33. Hardie, L. A. Dolomitization; a critical view of some current views. *Journal of Sedimentary Research* **57**, 166–183 (1987).

34. Hardie, L. A. Secular variation in seawater chemistry: An explanation for the coupled secular variation in the mineralogies of marine limestones and potash evaporites over the past 600 m.y. *Geology* **24**, 279–283 (1996).

35. Harrison, W. J. & Summa, L. L. Paleohydrogeology of the Gulf of Mexico Basin. *American Journal of Science* **291**, 109–176 (1991).

36. Hart, R. Chemical exchange between sea water and deep ocean basalts. *Earth and Planetary Science Letters* **9**, 269–279 (1970).

37. Hart, S. R., Erlank, A. J. & Kable, E. J. D. Sea floor basalt alteration: Some chemical and Sr isotopic effects. *Contr. Mineral. and Petrol.* **44**, 219–230 (1974).

38. Hart, S. R. & Staudigel, H. The control of alkalies and uranium in seawater by ocean crust alteration. *Earth and Planetary Science Letters* **58**, 202–212 (1982).

39. Hitchon, B., Billings, G. K. & Klovan, J. E. Geochemistry and origin of formation waters in the western Canada sedimentary basin—III. Factors controlling chemical composition. *Geochimica et Cosmochimica Acta* **35**, 567–598 (1971).

40. Hitchon, B. & Friedman, I. Geochemistry and origin of formation waters in the western Canada sedimentary basin—I. Stable isotopes of hydrogen and oxygen. *Geochimica et Cosmochimica Acta* **33**, 1321–1349 (1969).

41. Jones, G., Whitaker, F., Smart, P. & Sanford, W. Numerical modelling of geothermal and reflux circulation in Enewetak Atoll: implications for dolomitization. *Journal of Geochemical Exploration* **69–70**, 71–75 (2000).

42. Jones, G. D. Numerical analysis of seawater circulation in carbonate platforms: II. The dynamic interaction between geothermal and brine reflux circulation. *American Journal of Science* **304**, 250–284 (2004).

43. Jones, G. D. & Xiao, Y. Dolomitization, anhydrite cementation, and porosity evolution in a reflux system: Insights from reactive transport models. *Bulletin* **89**, 577–601 (2005).

44. Joye, S. B., MacDonald, I. R., Montoya, J. P. & Peccini, M. Geophysical and geochemical signatures of Gulf of Mexico seafloor brines. *Biogeosciences* **2**, 295–309 (2005).

45. Kadko, D., Baross, J. & Alt, J. The Magnitude and Global Implications of Hydrothermal Flux. in *Geophysical Monograph Series* (eds. Humphris, S. E., Zierenberg, R. A., Mullineaux, L. S. & Thomson, R. E.) 446–466 (American Geophysical Union, 2013). doi:10.1029/GM091p0446.

46. Kastner, M., Elderfield, H. & Martin, J. B. Fluids in convergent margins: what do we know about their composition, origin, role in diagenesis and importance for oceanic chemical fluxes? *Phil. Trans. R. Soc. Lond.* **335**, 243–259 (1991).

47. Keep, M., Harrowfield, M. & Crowe, W. The Neogene tectonic history of the North West Shelf, Australia. *Exploration Geophysics* **38**, 151–174 (2007).

48. Kohout, F. A. Cyclic flow of salt water in the Biscayne aquifer of southeastern Florida. *J. Geophys. Res.* **65**, 2133–2141 (1960).

49. Krassay, A. A. & Totterdell, J. M. Seismic stratigraphy of a large, Cretaceous shelf-margin delta complex, offshore southern Australia. *Bulletin* **87**, 935–963 (2003).

50. Kwon, E. Y. *et al.* Global estimate of submarine groundwater discharge based on an observationally constrained radium isotope model. *Geophys. Res. Lett.* **41**, 8438–8444 (2014).

51. Land, L. S. & Macpherson, G. L. Origin of Saline Formation Waters, Cenozoic Section, Gulf of Mexico Sedimentary Basin. *AAPG Bulletin* **76**, 1344–1362 (1992).

52. Lee, G. H., Lee, K. & Watkins, J. S. Geologic evolution of the Cuu Long and Nam Con Son basins, offshore southern Vietnam, South China Sea. *AAPG Bulletin* **85**, 1055–1082 (2001).

53. Leyden, R. & Bryan, G. M. Geophysical Reconnaissance on African Shelf: 2. Margin Sediments from Gulf of Guinea to Walvis Ridge. *Bulletin* **56**, (1972).

54. Locklair, R. E. & Lerman, A. A model of Phanerozoic cycles of carbon and calcium in the global ocean: Evaluation and constraints on ocean chemistry and input fluxes. *Chemical Geology* **217**, 113–126 (2005).

55. Luo, X., Dong, W., Yang, J. & Yang, W. Overpressuring mechanisms in the Yinggehai Basin, South China Sea. *Bulletin* **87**, 629–642 (2003).

56. Manheim, F. T. & Paull, C. K. Patterns of groundwater salinity changes in a deep continental-oceanic transect off the southeastern Atlantic coast of the U.S.A. *Journal of Hydrology* **54**, 95–105 (1981).

57. Mann, P. Passive Plate Margin. in *Encyclopedia of Marine Geosciences* (eds. Harff, J., Meschede, M., Petersen, S. & Thiede, J.) 1–8 (Springer Netherlands, 2014). doi:10.1007/978-94-007-6644-0_100-2.

58. Mark J. Osborne and Richard E. Swar. Mechanisms for Generating Overpressure in Sedimentary Basins: A Reevaluation. *Bulletin* **81 (1997)**, (1997).

59. Matthews, S. J., Fraser, A. J., Lowe, S., Todd, S. P. & Peel, F. J. Structure, stratigraphy and petroleum geology of the SE Nam Con Son Basin, offshore Vietnam. *Geological Society, London, Special Publications* **126**, 89–106 (1997).

60. Mello, U. T. & Karner, G. D. Development of Sediment Overpressure and Its Effect on Thermal Maturation: Application to the Gulf of Mexico Basin. *Bulletin* **80**, 1367–1396 (1996).

61. Michael, H. A. *et al.* Geologic influence on groundwater salinity drives large seawater circulation through the continental shelf: Geology Drives Seawater Circulation. *Geophys. Res. Lett.* **43**, 10,782-10,791 (2016).

62. Milliman, J. D. Production and accumulation of calcium carbonate in the ocean: Budget of a nonsteady state. *Global Biogeochem. Cycles* **7**, 927–957 (1993).

63. MOORE, D., DG, M., JR, C., RW, R. & FJ, E. Stratigraphic-seismic section 429 correlations and implications to Bengal Fan history. in *Initial reports of the Deep-Sea Drilling Project, Leg 22* (eds. von der Borch, C. C. & Sclater, J. G.) 403–412 (1974).

64. Moore, G. F., Saffer, D., Studer, M. & Pisani, P. C. Structural restoration of thrusts at the toe of the Nankai Trough accretionary prism off Shikoku Island, Japan: Implications for dewatering processes. *Geochemistry, Geophysics, Geosystems* **12**, 1–15 (2011).

65. Mottl, M. J. & Wheat, C. G. Hydrothermal circulation through mid-ocean ridge flanks: Fluxes of heat and magnesium. *Geochimica et Cosmochimica Acta* **58**, 2225–2237 (1994).

66. Mouchet, J.-P. & Mitchell, A. *Abnormal Pressures While Drilling: Origins, Prediction, Detection, Evaluation*. (Editions TECHNIP, 1989).

67. *Proceedings of the IODP, 313*. vol. 313 (Integrated Ocean Drilling Program, 2010).

68. Mudge, D. C. & Bujak, J. P. Eocene stratigraphy of the North Sea basin. *Marine and Pet roleum Geology* **11**, 166–181 (1994).

69. Müller, R. D., Dutkiewicz, A., Seton, M. & Gaina, C. Seawater chemistry driven by supercontinent assembly, breakup, and dispersal. *Geology* **41**, 907–910 (2013).

70. Nielsen, S. G. *et al.* Hydrothermal fluid fluxes calculated from the isotopic mass balance of thallium in the ocean crust. *Earth and Planetary Science Letters* **251**, 120–133 (2006).

71. Okiongbo, K. S. Volumetrics of Petroleum Generation: Implications for Expulsion and Overpressure. *Petroleum Science and Technology* **32**, 1257–1263 (2014).

72. Olsson, R. K., Gibson, T. G., Hansen, H. J. & Owens, J. P. Geology of the northern Atlantic coastal plain: Long Island to Virginia. in *The Atlantic Continental Margin* (1988).

73. Osborne, M. J. & Swarbrick, R. E. Mechanisms for Generating Overpressure in Sedimentary Basins: A Reevaluation. *AAPG Bulletin* **81**, (1997).

74. Pattier, F. *et al.* Mass Movements in a Transform Margin Setting: The Example of the Eastern Demerara Rise. in *Submarine Mass Movements and Their Consequences* (eds. Yamada, Y. et al.) 331–339 (Springer Netherlands, 2012). doi:10.1007/978-94-007-2162-3_30.

75. Paul, H. J., Gillis, K. M., Coggon, R. M. & Teagle, D. A. H. ODP Site 1224: A missing link in the investigation of seafloor weathering: ODP SITE 1224-SEAFLOOR WEATHERING. *Geochem. Geophys. Geosyst.* **7**, (2006).

76. Qin, X., Han, D.-H. & Zhao, L. Elastic characteristics of overpressures due to smectite-to-illite transition based on micromechanism analysis. *Geophysics* **84**, WA23–WA42 (2019).

77. Ramdhan, A. M. OVERPRESSURE AND COMPACTION IN THE LOWER KUTAI BASIN, INDONESIA. 329 (2010).

78. Reynaud, J.-Y. *et al.* ARCHITECTURE AND SEQUENCE STRATIGRAPHY OF A LATE NEOGENE INCISED VALLEY AT THE SHELF MARGIN, SOUTHERN CELTIC SEA. *Journal of Sedimentary Research* **69**, 351–364 (1999).

79. Riley, J. P. (John P. & Chester, R. (Roy). *Introduction to marine chemistry*. (Academic Press, 1971).

80. Roy, D. K., Ray, G. K. & Biswas, A. K. Overview of Overpressure in Bengal Basin, India. *Journal of The Geological Society of India* **75**, 644–660 (2010).

81. Sachse, V. F., Strozyk, F., Anka, Z., Rodriguez, J. F. & di Primio, R. The tectono-stratigraphic evolution of the Austral Basin and adjacent areas against the background of Andean tectonics, southern Argentina, South America. *Basin Res* **28**, 462–482 (2016).
82. Saffer, D. M. The permeability of active subduction plate boundary faults. *Geofluids* **15**, 193–215 (2015).
83. Saffer, D. M. & Bekins, B. A. Hydrologic controls on the morphology and mechanics of accretionary wedges. *Geology* **303**, 271–274 (2002).
84. Saffer, D. M. Pore pressure development and progressive dewatering in underthrust sediments at the Costa Rican subduction margin: Comparison with northern Barbados and Nankai: PORE PRESSURE AND DEWATERING. *J. Geophys. Res.* **108**, (2003).
85. Sanford, W. E., Whitaker, F. F., Smart, P. L. & Jones, G. Numerical Analysis of seawater on the frictional strength and sliding stability of intact marine mudstones. *American Journal of Science* **298**, 801–828 (1998).
86. Sass, A. M., Aass, H., Coolen, M. J. L., Cypionka, H. & Overmann, J. Microbial Communities in the Chemocline of a Hypersaline Deep-Sea Basin (Urania Basin, Mediterranean Sea). *Applied Environmental Microbiology* **67**, 5392–5402 (2003).
87. Schramm, B., Devey, C. W., Gillis, K. M. & Lackschewitz, K. Quantitative assessment of chemical and mineralogical changes due to progressive low-temperature alteration of East Pacific Rise basalts from 0 to 9 Ma. *Chemical Geology* **218**, 281–313 (2005).

88. Scott, T. M. A Geological Overview of Florida. *Florida Geological Survey Tallahassee* **50**, 1–80 (1992).

89. Seibold, E. & Hinz, K. Continental Slope Construction and Destruction, West Africa. in *The Geology of Continental Margins* (eds. Burk, C. A. & Drake, C. L.) 179–196 (Springer, 1974). doi:10.1007/978-3-662-01141-6_13.

90. Sheridan, R. E. & Grow, J. A. The Atlantic Continental Margin. (1988) doi:10.1130/DNAG-GNA-I2.

91. Shokes, R. F., Trabant, P. K., Presley, B. J. & Reid, D. F. Anoxic, Hypersaline Basin in the Northern Gulf of Mexico. *Science* **196**, 1443–1446 (1977).

92. Spencer, R. J. & Hardie, L. A. Control of seawater composition by mixing of river waters and mid-ocean ridge hydrothermal brines. *Fluid-Mineral Interactions* 409–419 (1990).

93. Stein, C. A. & Stein, S. Comparison of plate and asthenospheric flow models for the thermal evolution of oceanic lithosphere. *Geophys. Res. Lett.* **21**, 709–712 (1994).

94. Stoakes, F. A., Campbell, C. V., Cass, R. & Ucha, N. Seismic Stratigraphy Analysis of the Punta Del Este Basin, Offshore Uruguay, South America. *AAPG Bulletin* **75**, 219–240 (1991).

95. Suess, E. Marine cold seeps and their manifestations: geological control, biogeochemical criteria and environmental conditions. *Int J Earth Sci (Geol Rundsch)* **103**, 1889–1916 (2014).

96. Swarbrick, R. E. & Osborne, M. J. Mechanisms that generate abnormal pressures: an overview. in *Abnormal pressures in hydrocarbon environments: AAPG Memoir* vol. 70 13–14 (1998).

97. Taria, A., Hill, I. & Firth, J. Shipboard Scientific Party. Site 808. in *Proc. ODP, Init. Repts.* vol. 131 71–269 (1991).

98. Thompson, G. Basalt — Seawater Interaction. in *Hydrothermal Processes at Seafloor Spreading Centers* vol. 12 225–278 (Springer, 1983).

99. Van Cappellen, P. *et al.* Biogeochemical Cycles of Manganese and Iron at the Oxic−Anoxic Transition of a Stratified Marine Basin (Orca Basin, Gulf of Mexico). *Environ. Sci. Technol.* **32**, 2931–2939 (1998).

100. Vrolijk, P. On the mechanical role of smectite in subduction zones. *Geology* **18**, 703–707 (1990).

101. White, D. E., Hem, J. D. & Waring, G. A. Chemical composition of subsurface waters. *US Geological Survey Proffessional Papers* **440**, 67 (1963).

102. Wilson, A. M. Spatial patterns of diagenesis during geothermal circulation in carbonate platforms. *American Journal of Science* **301**, 727–752 (2001).

103. Wilson, A. M., Sanford, W., Whitaker, F. & Smart, P. Geothermal convection: a mechanism for dolomitization at Enewetak Atoll? *Journal of Geochemical Exploration* **69–70**, 41–45 (2000).

104. Wilson, A. M. & Garven, G. Paleohydrogeology of the San Joaquin basin, California. *Geological Society of America Bulletin* **111**, 432–449 (1999).

105. Wilson, A. M. The occurrence and chemical implications of geothermal convection of seawater in continental shelves. *Geophys. Res. Lett.* **30**, 2127 (2003).

106. Wilson, A. M. Fresh and saline groundwater discharge to the ocean: A regional perspective. *Water Resour. Res.* **41**, 11 (2005).

107. Xinong, X., Sitian, L., Weiliang, D. & Qiming, Z. Overpressure Development and Hydrofracturing in the Yinggehai Basin. *J Petroleum Geol* **22**, 437–454 (1999).

108. Yu, H. & Hilterman, F. J. The effect of pressure on rock properties in the Gulf of Mexico: Comparison between compaction disequilibrium and unloading. *Interpretation* **2**, SB1–SB15 (2014).

109. Zhao, J., Li, J. & Xu, Z. Advances in the origin of overpressures in sedimentary basins. *Petroleum Research* **3**, 1–24 (2018).

APPENDIX A

EXAMPLE BRINE FLUID CONCENTRATIONS

Table A.1 Example Brine Fluid Concentrations

	Salinity	**[Cl^-]**	**[Na^+]**	**[K^+]**	**[Ca^{2+}]**	**[Mg^{2+}]**	**Reference**
Gulf of Mexico							
Bottom Water	34	564	462	43	11	11	*Joye*, 2005
GC233	121	2090	1751	22	36	9.7	*Joye*, 2005
GB425	130	2110	1790	89	59	8.7	*Joye*, 2005
Orca Basin	258	5000	n.d	n.d	32	n.d	*Shokes et al*, 1977
Orca Basin	250	4450	4240	17.2	29	42.4	*Van Cappellen et al.*, 1998
Mediterranean							
Bottom Water	35	600	492	11.2	11	56	*Charlou et al.*, 2003
Urania basin	200	2830	n.d	n.d	34	n.d	*Sass et al.*, 2001
Libeccio Basin	321	5333	n.d	n.d	21		*Sass et al.*, 2001
Tyro basin	n.d	5350	n.d	n.d	34	n.d	*Sass et al.*, 2001
Napoli	82	1380	1347	8.1	8.4	33.9	*Charlou et al.*, 2003
Nadir	120	1979	1884	7.2	22.2	27.9	*Charlou et al.*, 2003
Urania	70	1075	922	26.6	16.8	82.3	*Charlou et al.*, 2003
Red Sea							
Shaban Deep #3	242	4358	4408	44	20	77	*Eder et al.*, 2002
Shaban Deep #12	220	4361	3953	39	19	74	*Eder et al.*, 2002

Salinity = ‰.
Other ions = mM

APPENDIX B

FLUID COMPOSITION ADJUSTMENT

Table B.1 Fluid Composition Adjustment Process

	Ca^{2+}	K^{+}	Mg^{2+}	Na^{+}	Cl^{-}
			Type 3		
1	2260.8	211.6	549.7	2097.6	5132.8
2	241.3	22.6	58.7	223.9	547.9
3	20.6	10.3	106.6	469.7	547.9
4	220.7	12.3	-48.0	-245.8	0
5	110.4	12.3	-24.0	-245.8	0
			MOR		
6	76.3	37.3	1.3	418	532.3
7	78.5	38.39314	1.3	430.3	547.9
8	20.6	10.3	106.6	469.7	547.9
9	57.9	28.1	-105.2	-39.4	0
10	29.0	28.1	-52.6	-39.4	0

1 — Original Type 3 brine fluid (meq/l)
2 — Adjust to Seawater Cl^{-}
3 — Seawater
4 — Net Fluid Flux
5 — Net Flux in (mmol/l)
6 — MOR composition (meq/l)
7 — Adjust to Seawater Cl^{-}
8 — Seawater
9 — Net MOR Flux
10 — Net Flux in (mmol/l)

The table above details the step-by-step calculations for adjusting fluid compositions using the method of Spencer and Hardie (1990), using the examples of MOR hydrothermal fluid and our Type 3 brine. The ion concentrations are converted to meq/l initially, then adjusted to seawater chlorinity and the concentrations of seawater are subtracted out. Concentrations are converted to mmol/l in the final step.

APPENDIX C

LOWER-BOUND GLOBAL MASS FLUXES AND FLUX RATIOS

Table C.1 Lower-Bound Global Mass Fluxes and Flux Ratios

	Ca^{2+}	K^{+}	Mg^{2+}	Na^{+}
1 — Cold Seeps	-4.47E+08	2.52E+08	-3.41E+09	2.10E+09
2 — Clastic-Derived	2.57E+09	-3.92E+08	-2.14E+09	-1.61E+09
3 — $CaCl_2$ Brines	1.29E+10	1.40E+09	-1.70E+09	-1.65E+10
4 — Carbonate-Derived	5.97E+08	-1.10E+08	-9.53E+08	1.49E+09
5 — Cold Seeps	-	42	4.1	-
6 — Clastic-Derived	9.2	15	18	33
7 — $CaCl_2$ Brines	-	220	43	930
8 — Carbonate-Derived	-	140	-	500

1—4 minimum mass flux estimates (kg/yr); 5—8 volumetric flux ratios assuming the minimum global independent volumetric flux from passive margins (5.8E+08)

APPENDIX D

ORIGINAL COMPOSITIONS OF DEEP $CaCl_2$ BASINAL BRINES

Table D.1 Original Compositions of Deep $CaCl_2$ Basinal Brines

	[Ca^{2+}]	**[K^+]**	**[Mg^{2+}]**	**[Na^+]**	**[Cl^-]**	**Reference**
GoM	36400	538	1730	59500	158200	[1]
	34000	7080	3920	79000	198700	[1]
	10600	1000	1232	73550	142725	[2]
Michigan	70100	13200	6970	21900	188000	[3]
	94900	12100	14700	21300	256000	[3]
Illinois	11100	2160	2300	61000	122000	[3]
	22400	1380	2840	49000	125000	[3]
Dead Sea	82865	28730	19765	20515	265150	[4]

[1] *Carpenter et al.* (1974), [2] Table 13 in *White et al*. (1963), [3] *Graf et al*. (1966), [4] *Bentor* (1969)

All data collected from Table 8, (*Hardie*, 1991)